

# Spin Hall effect in Rashba-Dresselhaus planar strips in the presence of electron correlations

José A. Riera

*Instituto de Física Rosario, Consejo Nacional de Investigaciones Científicas y Técnicas,  
and Universidad Nacional de Rosario, Rosario, Argentina*

(Dated: November 5, 2021)

A model with both Rashba and Dresselhaus spin orbit (SO) couplings and Hubbard electron-electron interaction is studied on planar strips at quarter filling at zero temperature in the clean limit. In the absence of Hubbard repulsion and at equilibrium, within linear response theory, a nonmonotonic behavior of the spin Hall conductivity as a function of the ratio of the Rashba ( $\alpha$ ) and Dresselhaus ( $\beta$ ) strengths was found for large enough SO strengths. This behavior is signalled by a peak or a cusp, depending on the strip width, at intermediate values of  $\beta/\alpha$  in the interval  $[0, 1]$ . This behavior of the spin Hall conductivity was correlated with the one for the longitudinal spin conductivity. This study was then extended to the out-of-equilibrium regime that arises by imposing a finite voltage bias between the two ends of an open strip. This system, in the presence of a Hubbard term with coupling  $U$ , was treated with the density matrix renormalization group technique and with the Landauer-Buttiker formalism. It was found that relevant properties to the spin Hall effect, such as the transversal spin current and the spin accumulation, present a similar nonmonotonic behavior as the one found for the spin conductivities. More importantly, it was also found that these properties are enhanced by the repulsive Hubbard interaction up to a moderate value of  $U$ .

## I. INTRODUCTION

The flow of spins in solids has recently received an intense interest both because it manifests at a fundamental level in the field of topological insulators [1] and also because it may lead to technological applications in spintronics [2–4]. Particularly important is the case when the spin flow is generated by itinerant spin-orbit interactions (SOI) of the Rashba or Dresselhaus forms.

In bulk inversion asymmetric (BIA) systems the SOI effectively leads to the (linear) Dresselhaus spin-orbit coupling (DSOC) [5]:

$$H_{BIA} = \beta(\sigma_x k_x - \sigma_y k_y) \quad (1)$$

In most materials, this linear in momentum DSOC is accompanied by a term which is cubic in momentum but it will not be included in the present study. On the other hand, the structure inversion asymmetry (SIA), which is due to the presence of surfaces or interfaces, the SOI gives rise at an effective level to the Rashba spin-orbit coupling (RSOC) [6, 7] defined by the Hamiltonian:

$$H_{SIA} = \alpha(\sigma_x k_y - \sigma_y k_x) = \alpha \boldsymbol{\sigma} \cdot [\mathbf{k} \times \mathbf{z}] \quad (2)$$

The RSOC has the important property of being able to be tuned by an external electric field in addition to its value determined by the intrinsic properties of the system.

In most materials, both Rashba and Dresselhaus SOI are present, and their relative strength can be determined using magneto-transport properties [8, 9], particularly by measuring the beating patterns in Shubnikov-de Haas oscillations [10]. The presence of both types of SOI in a given system depends on the atomic structure of the material involved but also on the direction on which the wires are grown [11]. The electric fields implied in the lateral confinement that is frequently used to define a

strip can also modify the ratio between the RSOC and DSOC strengths [11, 12].

Both Rashba and Dresselhaus SOI lead to the spin Hall effect but their effects interfere and interesting physics appears when the RSOC and DSOC strengths,  $\alpha$  and  $\beta$ , are varied. The most interesting magnetic state is the so-called persistent spin helix (PSH) [13], which appears when both Rashba and Dresselhaus are present with equal strength. In addition, at the PSH point, D'yakonov-Perel and Elliott-Yafet spin-flip processes due to non-magnetic impurities are suppressed, thus enabling non-ballistic transport [14–16]. A clear signature of the persistent helix state was detected as a dip in the magnetoconductance [17].

For arbitrary values of the ratio  $\beta/\alpha$ , the interband contribution to the longitudinal optical conductivity was examined for the isotropic two-dimensional (2D) system with a parabolic band in the clean limit [18], and it was found that it disappears when  $\alpha = \beta$ . The spin Hall conductivity was originally computed for the pure Rashba model on the infinite plane for a parabolic band [19, 20]. This quantity was also computed for arbitrary values of  $\alpha, \beta$ , and it was found to be  $\sigma_{sH} = \frac{1}{8\pi^2} \gamma_{\pm}$  (in our units of  $e = 1$ ) [21], where  $\gamma_{\pm} = \text{sign}(\alpha^2 - \beta^2)$  is the Berry phase. That is,  $\sigma_{sH} = \frac{1}{8\pi}$  in the interval  $0 \leq \beta/\alpha < 1$ .

Although most of the previous theoretical work has been done in the isotropic 2D system, actual spintronics devices involve finite width conductors or wires, and taking into account the nanoelectronics drive towards smaller wire widths, it is of fundamental importance to study the behavior of the relevant magneto-transport properties for the smallest possible widths. The relatively few studies on anisotropic 2D systems were performed using electrostatic lateral confinement. In those works various finite size effects were analyzed both theo-

retically [14, 22] and experimentally [17, 23, 24].

The final ingredients for the model to be studied in the present work come from emergent phenomena at oxide interfaces, particularly  $\text{LaAlO}_3/\text{SrTiO}_3$  where RSOC is present [26–33]. While for conventional semiconductor materials where spin-orbit effects were studied, typically small electron fillings were considered, these new materials motivate the research at larger electron fillings, where electron correlations become more relevant and various magnetic orderings induce complex transport behaviors.

The simplest and perhaps more interesting way of considering electron-electron correlations is adding to the tight-binding Hamiltonian the on-site Hubbard term. There are various studies of models including SO and Hubbard interactions in one- and two- dimensions. Most of these studies have only considered the Rashba SOC [34–37] but there are also studies where both RSOC and DSOC were involved [38].

In the present work, various magneto-transport properties, particularly those related to the spin-Hall effect, will be studied on finite strips with Rashba and Dresselhaus SOI, in the presence of electron-electron Hubbard interaction, in the whole range of parameters  $0 \leq \beta/\alpha \leq 1$ , and for electron filling  $n = 0.5$ . These strips have atomically defined open edges, that is, they are not regions of a 2D system laterally delimited by voltage gates. Hence, the considered values of the Rashba and Dresselhaus SOI are intrinsic to the material of the strip. This study will only consider clean systems.

The study of this model in out of equilibrium and interacting regimes will be performed using computational techniques, the density matrix renormalization group technique, and the Landauer-Buttiker formalism. Although there are previous studies of channels at particular values of the Rashba and Dresselhaus SO couplings as a function of the applied voltage bias by the Landauer formalism [25], a systematic study as a function of these couplings, as well as including electron correlation effects, is still lacking.

This paper is organized as follows. In Sec. II the second quantized model to be studied is defined, and the main theoretical methods employed are outlined. In Sec. III the study of the equilibrium non-interacting case is studied in linear response. In Sec. IV the out of equilibrium interacting two-chain strip is studied using density matrix renormalization group. In Sec. V the out of equilibrium system is studied within the Landauer-Buttiker formalism. Finally, in the Conclusions, the main results obtained are emphasized and their possible relevance to spintronics devices is discussed.

## II. MODEL AND METHODS

The Hamiltonian to be studied in the present work can be expressed as  $H = H_h + H_R + H_D + H_U$ , where  $H_h$

corresponds to the usual hopping term:

$$H_h = -t \sum_{\langle l, m \rangle, \sigma} (c_{l,\sigma}^\dagger c_{m,\sigma} + H.c.) \quad (3)$$

The Rashba SO Hamiltonian on the square lattice in the  $\{x, y\}$ -plane is given by [34, 39–41]:

$$H_R = \alpha \sum_l [c_{l+x,\downarrow}^\dagger c_{l,\uparrow} - c_{l+x,\uparrow}^\dagger c_{l,\downarrow} + i(c_{l+y,\downarrow}^\dagger c_{l,\uparrow} + c_{l+y,\uparrow}^\dagger c_{l,\downarrow}) + H.c.] \quad (4)$$

and the Dresselhaus SO term is similarly given by (Appendix A):

$$H_D = \beta \sum_l [c_{l+y,\downarrow}^\dagger c_{l,\uparrow} - c_{l+y,\uparrow}^\dagger c_{l,\downarrow} + i(c_{l+x,\downarrow}^\dagger c_{l,\uparrow} + c_{l+x,\uparrow}^\dagger c_{l,\downarrow}) + H.c.] \quad (5)$$

The last term of  $H$  corresponds to the Hubbard interaction:

$$H_U = U \sum_l n_{l,\uparrow} n_{l,\downarrow} \quad (6)$$

where the notation is conventional.

The total Hamiltonian  $H$  will be studied on strips of length  $L$  in the longitudinal  $x$ -direction and width  $W$  in the transversal  $y$ -direction, with  $W < L$ . Open boundary conditions (BC) are imposed on the transversal direction.

In the following, the normalizations  $\sqrt{\alpha^2 + \beta^2} = V_{SO}$  and  $\sqrt{t^2 + V_{SO}^2} = 1$ , which will be the scale of energy, have been adopted. These two normalizations are essential to compare quantities for different ratios of  $\alpha$  and  $\beta$  for a fixed value of  $V_{SO}/t$ , as is the purpose of the present study. For example, with these normalizations, the relative difference in total energy for  $W = 8$ ,  $V_{SO}/t = 0.5$ , in the whole range of  $0 \leq \beta/\alpha \leq 1$ , with  $U = 0$ , is less than 0.023 %, much smaller than the relative differences obtained for the physical quantities studied. In the same way, the total energy is approximately constant as  $V_{SO}/t$  is varied for a fixed value of  $\beta/\alpha$ .

In the noninteracting case ( $U = 0$ ) the main quantity that will be studied is the spin-Hall conductivity,  $\sigma_{sH}$ . At equilibrium, in linear response,  $\sigma_{sH}$  is defined as the zero frequency limit of the spin-charge transversal response function at zero temperature [19, 20]:

$$\sigma_{xy}^{sc}(\omega) = -i \frac{1}{\pi N} \sum_n \sum_m \frac{\langle \Psi_n | \hat{j}_y^s | \Psi_m \rangle \langle \Psi_m | \hat{j}_x | \Psi_n \rangle}{[(E_n - E_m)^2 - \omega^2]} \quad (7)$$

where  $\hat{j}_x$  is the longitudinal charge current operator and  $\hat{j}_y^s$  is the transversal spin current operator. The charge current operator can be written as the sum of two terms,  $\hat{j}_{hop,x}$  and  $\hat{j}_{SO,x}$ , usually referred to as the spin-conserving and spin-flipping currents, respectively (see Appendix B). Similarly, the spin currents can be written as  $\hat{j}_y^s = \hat{j}_{hop,y}^s + \hat{j}_{SO,y}^s$ .

In linear response, a measure of the spin current in the longitudinal direction is given by the longitudinal spin conductivity  $\sigma_{xx}^s$ , which is defined as the zero frequency limit of a response function analogous to the one given by Eq. (7) except that the operator of the transversal spin current  $\hat{j}_y^s$  is replaced by the operator of the longitudinal spin current  $\hat{j}_x^s$ . Similarly, the anomalous Hall conductivity  $\sigma_{AH}$  corresponds to the zero frequency limit of a response function obtained from Eq. (7) by replacing  $\hat{j}_y^s$  by the transversal charge current operator  $\hat{j}_y$ .

Of particular interest is the contribution from the spin-flipping currents to the Drude peak, which will also be computed in linear response. The hopping and SO contributions to the Drude weight are defined as [42]:

$$\frac{D_a}{2\pi} = \frac{K_{a,x}}{2N} - I_{reg,a} \quad (8)$$

$a = hop, SO$ , where  $K_{hop,x} = -\langle (H_h)_x \rangle$ ,  $K_{SO,x} = -\langle (H_R + H_D)_x \rangle$ , and

$$I_{reg,a} = \frac{1}{N} \sum_{n \neq 0} \frac{|\langle \Psi_n | \hat{j}_{a,x} | \Psi_0 \rangle|^2}{E_n - E_0} \quad (9)$$

are the corresponding contributions to the regular part of the longitudinal optical conductivity. Notice that the total  $I_{reg}$ , and hence the total Drude weight, is the sum of the hopping and SO contributions, and the contribution that results from the product of the matrix elements of  $\hat{j}_{SO,x}$  and  $\hat{j}_{hop,x}$ . For all the parameters considered in the present effort, this mixing contribution is negligible [43].

Linear response results were obtained for strips with periodic BC along the longitudinal direction by exact numerical diagonalization of the Hamiltonian in momentum space (Appendix A).

The study of out-of-equilibrium regimes, and in the presence of the Hubbard interaction, is performed, for  $W = 2$  strips, by using the time-dependent density matrix-renormalization group (td-DMRG) method [44–46]. In this case, a small finite voltage bias,  $\Delta V$ , is imposed at the strip ends at time  $\tau = 0$ , after the ground state has been properly described at equilibrium. This setup is schematically shown in Fig. 4(a) below. This technique has been already employed to study two- and three-chains Rashba-Hubbard strips [34, 37].

In general, the time evolution of an arbitrary operator  $\hat{O}$ , is given by  $O(\tau) = \langle \Psi(\tau) | \hat{O} | \Psi(\tau) \rangle$ , where  $|\Psi(\tau)\rangle$  is the time-evolved ground state. The procedure follows the so-called "static" algorithm [44] and at each time step the time evolution operator is applied as a series expansion involving up to the 40-th order. Then, the time-evolution of several physical properties, such as charge and spin currents, can be computed. The hopping contribution to the longitudinal charge current is directly computed from the operator  $\hat{j}_{hop,x}$ , and the total longitudinal current is computed as the time derivative of the charge occupation of one half of the strip.

Although some qualitative features can be inferred by simple inspection of  $O(\tau)$  plots, for a more quantitative statement it is necessary to assign a single number to each physical property for any set of parameters  $\beta/\alpha$ ,  $V_{SO}/t$ , and  $W$ . Following Refs. [44–46] this single number corresponds to the amplitude of the time oscillation that follow each physical property due to the finite length of the system. That is,  $O = \text{amplitude}(O(\tau))$ . Further details will be provided in Sec. IV.

In addition to transversal spin currents, another quantity related to the spin Hall effect is the spin accumulation defined as:

$$\Delta S^z = S_{e1}^z - S_{e2}^z \quad (10)$$

where:

$$S_{e1}^z = \sum_{i=1,w} S^z(i)$$

$$S_{e2}^z = \sum_{i=1,w} S^z(W - w + 1)$$

where  $S^z(i)$  is the total  $z$ -magnetization of leg  $i$  ( $i = 1, \dots, W$ ), and  $w = \max(1, W/4)$ .

An alternative approach, suitable to study wider strips, is the Landauer-Buttiker approach, which deals with the transmission of an electron wavepacket through a finite "scattering region", described by the total Hamiltonian  $H$  ( $U = 0$ ) connected to two semi-infinite leads (horizontal leads in Fig. 7(a)) described by  $H_h$ . A small voltage bias  $\Delta V = 0.1$  is applied between these two semi-infinite leads. Calculations within this approach are performed using the Kwant package [47] at zero temperature and at quarter filling, which is imposed by appropriately setting the Fermi level of the central, scattering region [48]. Rather than computing conductances, a procedure giving microscopic quantities such as the  $x, y, z$ -components of the spin at each site and the charge and spin currents between each nearest neighbor pair of sites, was adopted [49, 50]. These quantities are obtained by taking the quantum averages of the corresponding operators over the scattering wave function on the scattering region. In order to compute the spin accumulation and the transversal spin currents averaged over a region at the strip edge, a four-terminal setup is used (Fig. 7(a)). The vertical semiinfinite leads are also described by  $H_h$ . The code has been checked by verifying that the spin currents and  $\langle S_l^z \rangle$ ,  $l = 1 \dots N$  (and hence the spin accumulation) vanish at the  $\beta = \alpha$  point, and also at this point  $\langle S_l^x \rangle = \langle S_l^y \rangle$  due to the restoring of the  $U(1)$  symmetry. In addition, by interchanging  $\alpha$  and  $\beta$ , the same results are obtained with reversed sign for the transversal spin currents and  $\langle S_l^z \rangle$ .

For the interacting case,  $U > 0$ , a simple Hartree-Fock decoupling is implemented and at each site the values of  $\langle n_\uparrow \rangle$ ,  $\langle n_\downarrow \rangle$ , are provided by independent variational Monte Carlo simulations involving a single Gutzwiller factor for the Hubbard repulsion  $U$  [37, 51]. Additional details of the calculation of these properties are provided in Sec. V.

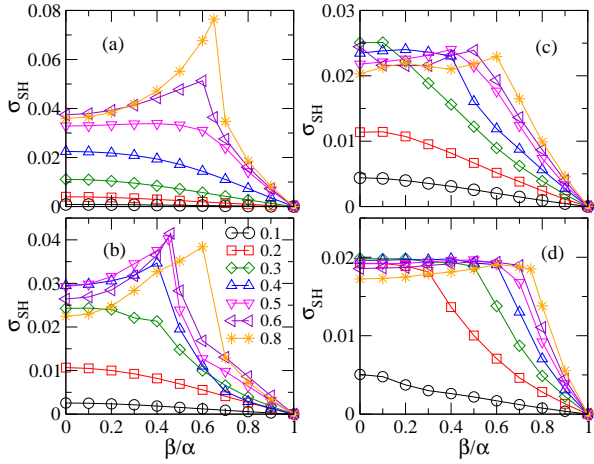


FIG. 1. (Color online) Spin Hall conductivity as a function of  $\beta/\alpha$ , for various  $V_{SO}/t$  indicated on the plot, (a)  $W = 2$ , (b)  $W = 4$ , (c)  $W = 8$ , and (d)  $W = 32$ .

### III. NONINTERACTING STRIPS, LINEAR RESPONSE

Let us start with the noninteracting case,  $U = 0$ , at equilibrium. All the results shown in the present section were obtained for strips of length  $L = 2000$  with periodic BC in the longitudinal direction.

Results for the spin Hall conductivity  $\sigma_{SH}$ , obtained using Eq. (7), as a function of  $\beta/\alpha$  for various strip widths  $W$  and SOI strengths  $V_{SO}/t$  are shown in Fig. 1. For all the strip widths and  $V_{SO}/t$  considered,  $\sigma_{SH}$  presents a finite value at the Rashba point ( $\beta = 0$ ) and vanishes at the PSH point ( $\beta = \alpha$ ). This latter result is expected because  $\sigma_{SH}$  reverses its sign when the values of  $\beta$  and  $\alpha$  are interchanged. For small values of  $V_{SO}/t$  and small  $W$ , the expected monotonic decrease of  $\sigma_{SH}$  as  $\beta/\alpha$  varies from zero to one is observed.

However, as it can be seen in Fig. 1(a) for  $W = 2$ , there is an unexpected nonmonotonic behavior as  $\beta/\alpha$  increases from zero to one for large values of  $V_{SO}/t$ . This nonmonotonic behavior is one of the main results of this work. For  $W = 2$  it is signalled by the presence of a peak in  $\sigma_{SH}$  at an intermediate value of  $\beta/\alpha$ ,  $R^* \approx 0.6$ , for  $V_{SO}/t \gtrsim 0.6$ . For  $W = 4$ , (Fig. 1(b)) this peak is already present for  $V_{SO}/t \geq 0.4$ , although a small cusp can be observed for  $V_{SO}/t = 0.3$ . The position of the peak  $R^*$  moves from  $\approx 0.4$  to  $\approx 0.6$  as  $V_{SO}/t$  increases.

The peak in  $\sigma_{SH}$  at  $R^*$ , for the same value of  $V_{SO}/t$ , is most intense for  $W = 2$ , and it becomes less pronounced as the strip width is increased. Although the peak is still present for  $W = 8$  (Fig. 1(c)), it has mostly disappeared and changed into a cusp for  $W = 32$  (Fig. 1(d)). For  $W = 64$ , results are virtually indistinguishable from those of  $W = 32$ . For  $W \geq 32$ ,  $\sigma_{SH}$  becomes approximately constant in the interval  $0 \leq \beta/\alpha \leq 1 - \epsilon$ , with  $\epsilon \rightarrow 0$  for  $V_{SO}/t \rightarrow \infty$ .

It is also important to remark that this peak or cusp in

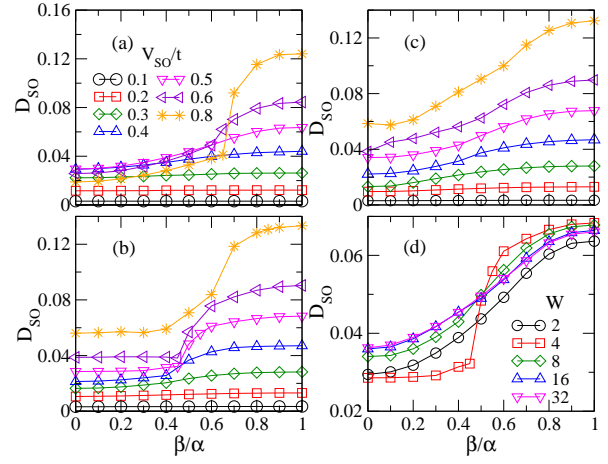


FIG. 2. (Color online) Spin-flipping contribution to the Drude peak,  $D_{SO}$ , as a function of  $\beta/\alpha$ , for various  $V_{SO}/t$  indicated on the plot, (a)  $W = 2$ , (b)  $W = 4$ , (c)  $W = 8$ . (d)  $D_{SO}$  for  $V_{SO}/t = 0.5$ , and various strip widths  $W$  indicated on the plot.

$\sigma_{SH}$  separates two clearly different regimes with different curvatures for  $\beta/\alpha$  below or above its position  $R^*$ .

By replacing the two contributions to both charge and spin currents, as discussed in the previous section, into the integrand of Eq. (7), it turns out that there are four possible contributions to  $\sigma_{SH}$ . For strips with periodic BC on the longitudinal  $x$  direction, only the contribution from the product of the matrix elements of  $\hat{j}_{SO,x}$  and  $\hat{j}_{hop,y}^s$  is different from zero for all values of  $\beta/\alpha$ ,  $V_{SO}/t$  and  $W$  considered, thus extending the previous result for the pure Rashba model [42]. This behavior also holds when open BC are adopted in the longitudinal direction for sufficiently long chains, but as the length  $L$  is reduced, other contributions become sizable particularly the one involving the product of the matrix elements of  $\hat{j}_{hop,x}$  and  $\hat{j}_{hop,y}^s$ .

Since the spin-flipping part of the longitudinal charge current is correlated with the hopping part of the transversal spin to produce a finite value of the spin Hall conductivity, it is interesting to examine how  $\hat{j}_{SO,x}$  correlates with the operators involved in other physical properties as a function of  $\beta/\alpha$ .

Let us study in the first place the contribution of  $\hat{j}_{SO,x}$  to the Drude peak, as defined in Sec. II. Results for various strip widths and SOI strengths  $V_{SO}/t$  are shown in Fig. 2. A general trend of increasing  $D_{SO}$  with  $\beta/\alpha$  for a given  $V_{SO}/t$  and  $W$  can be observed. For a fixed  $W$  and  $\beta/\alpha$ , there is also a general increase of  $D_{SO}$  with  $V_{SO}/t$ , as expected, with the exception of  $W = 2$  and  $V_{SO}/t \gtrsim 0.6$ , for small values of  $\beta/\alpha$ , as it can be observed in Fig. 2(a). More relevant for the discussion of the spin Hall conductivity is the presence of a jump in  $D_{SO}$  at the value of  $\beta/\alpha = R^*$  at which there is a peak in  $\sigma_{SH}$  for the corresponding values of  $V_{SO}/t$ , for  $W = 2$  and  $4$ , as it can be seen in Figs. 2(a) and 2(b). In con-

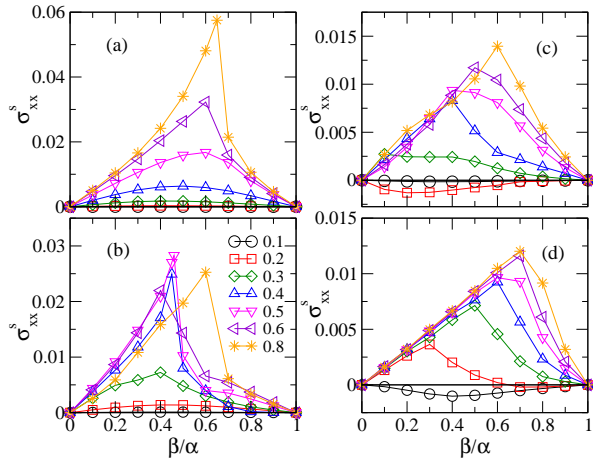


FIG. 3. (Color online) Longitudinal spin conductivity as a function of  $\beta/\alpha$ , for various  $V_{SO}/t$  indicated on the plot, (a)  $W = 2$ , (b)  $W = 4$ , (c)  $W = 8$ , and (d)  $W = 32$ .

trast, for  $W = 8$ , consistently with the smoothing out of the peaks in  $\sigma_{sH}$ , the jumps are replaced by an inflection point for the corresponding values of  $V_{SO}/t$ , as shown in Fig. 2(c). The dependence of  $D_{SO}$  with  $\beta/\alpha$  for  $W \gtrsim 16$  becomes increasingly smooth as  $W$  is increased. In order to make this behavior more apparent,  $D_{SO}$  was replotted in Fig. 2(d) for a single value of  $V_{SO}/t = 0.5$ , and various values of  $W$ . It is also noticeable that the dependence with  $W$  is already saturated for  $W \approx 32$ .

In the second place, let us examine the contribution of  $\hat{j}_{SO,x}$  to another magneto-transport effect due to the SOI that is the longitudinal spin conductivity  $\sigma_{xx}^s$ , which is the linear response corresponding to the spin polarized current to be studied in the next sections.

Results for the longitudinal spin conductivity for various values of  $W$  and  $V_{SO}/t$  as a function of  $\beta/\alpha$  are shown in Fig. 3. First, notice that this quantity vanishes at the pure Rashba and at the pure Dresselhaus points, which is a well-known result [53, 54]. As expected for the same argument as for the spin Hall conductivity,  $\sigma_{xx}^s$  also vanishes at  $\beta = \alpha$ . For  $W = 2$  (Fig. 3(a)),  $\sigma_{xx}^s$  acquire finite values by increasing  $\beta/\alpha$  reaching a maximum at an intermediate point. This dependence is smooth for small values of  $V_{SO}/t$ . For  $V_{SO}/t \geq 0.6$ , a sharp peak appears separating two regions with quite different slopes. A similar behavior can be observed for  $W = 4$  (Fig. 3(b)). For  $W = 2$  and 4, the smooth behavior of  $\sigma_{xx}^s$  occurs for the same values of  $V_{SO}/t$  for which a smooth behavior is present in  $\sigma_{sH}$ , and for large  $V_{SO}/t$ , the cusps occur also at the same values  $R^*$  as the cusps in  $\sigma_{sH}$  for the same  $V_{SO}/t$ , as seen in Figs. 1(a) and 1(b).

This correspondence between the behaviors of  $\sigma_{sH}$  and  $\sigma_{xx}^s$ , for the same values of  $V_{SO}/t$  and  $W$ , suggests that the latter could be obtained from the former by subtracting a quantity that decreases linearly from its maximum value at  $\beta = 0$  to zero at the PSH point. For large strip widths, as shown in Figs. 3(c) and 3(d) for  $W = 8$  and 32

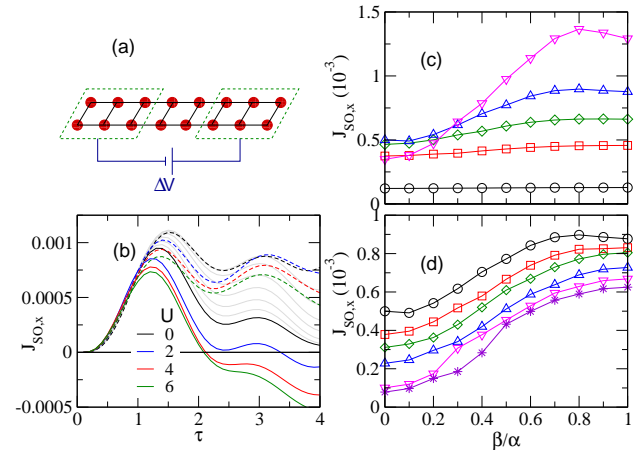


FIG. 4. (Color online) (a) Schematic picture of the td-DMRG setup. (b) Time evolution of the longitudinal SO or spin-flipping charge current,  $J_{SO,x}$ , for  $U = 0, 2, 4$  and  $6$ ,  $\beta = 0$  (full lines) and  $\beta = \alpha$  (dashed lines),  $V_{SO}/t = 0.6$ . In (b), results for  $U = 0$  and  $\beta/\alpha = 0.2, 0.3, 0.4, 0.5, 0.6$ , and  $0.7$  (from bottom to top) are shown with grey lines. (c) Amplitude of  $J_{SO,x}$  (see text), as a function of  $\beta/\alpha$ , for  $V_{SO}/t = 0.2$  (circles),  $0.4$  (squares),  $0.5$  (up triangles),  $0.6$  (diamonds), and  $0.8$  (down triangles),  $U = 0$ . (d) Amplitude of  $J_{SO,x}$  as a function of  $\beta/\alpha$ , for  $V_{SO}/t = 0.6$ , and  $U = 0, 1, 2, 4, 6$ , and  $8$ , from top to bottom. Results obtained with td-DMRG on the  $24 \times 2$  cluster.

respectively,  $\sigma_{xx}^s$  presents a well defined linear behavior for small  $\beta/\alpha$  that extends up to a value  $1 - \epsilon$ , where  $\epsilon$  is equal to the value described above for  $\sigma_{sH}$  for the same  $V_{SO}/t$  and  $W$ . Hence, these behaviors for large  $W$  and  $V_{SO}/t$  gives further support to the previous suggestion that  $\sigma_{xx}^s$  and  $\sigma_{sH}$  differ by a linear function decreasing from  $\beta = 0$  to  $\beta = \alpha$ .

Let us now come back to the previous discussion about the role of  $\hat{j}_{SO,x}$ . As for the  $\sigma_{sH}$  case, the integrand in  $\sigma_{xx}^s$  can be split in four contributions, and again the solely nonvanishing contribution turns out to be the one involving the matrix elements of  $\hat{j}_{SO,x}$ , this time multiplied by the matrix elements of  $\hat{j}_{hop,x}^s$ . This fact emphasizes the central role played by the longitudinal spin flipping current  $\hat{j}_{SO,x}$  in the two most relevant effects of itinerant SOI.

Just for completeness, and partially for checking purposes, the anomalous Hall conductivity, extending the well-known result for the pure Rashba model [52], was found to vanish for all values of  $V_{SO}/t$ ,  $W$ , and  $\beta/\alpha$  considered.

#### IV. OUT OF EQUILIBRIUM REGIME

As mentioned in Sec. II, it is necessary to resort to techniques such as td-DMRG to study properties in out of equilibrium regimes and in the presence of electron-electron interactions. In the present section, td-DMRG

is applied only to the  $W = 2$  strip, specifically to the  $24 \times 2$  system at  $n = 0.5$ . Most results were obtained by retaining 600-700 states in the truncation stage. A schematic illustration of the computational setup is shown in Fig. 4(a). The voltage bias  $\Delta V = 0.01$  is applied at time  $\tau = 0$  to the two halves of the system.

Typical td-DMRG time-evolution results for the SO contribution to the longitudinal charge current,  $J_{SO,x}$ , are provided in Fig. 4(b). This quantity was selected because it corresponds to the operator  $\hat{j}_{SO,x}$ , which plays an essential role in the behavior of relevant properties in linear response, as discussed in the previous section. In addition, between the components of the total longitudinal current  $J_x$ ,  $J_{SO,x}$  is the one that has the strongest dependence with  $\beta/\alpha$ , as it can be observed in Fig. 4(b) for  $V_{SO}/t = 0.6$ , and for various values of  $U$ .

As described in Sec. II, the value of each quantity for each set of parameters is adopted as the amplitude of its time evolution. As it can be seen in Fig. 4(b), for most properties, this time evolution presents at small times a double peak structure, although in some cases one of the peaks appears as a shoulder. Due to the relatively few states retained, and the algorithm adopted, only the results at short times are reliable. Then, by convention, the amplitude is defined as the average of the time evolution between those first two peaks.

Results for  $J_{SO,x}$  as a function of  $\beta/\alpha$  for various values of  $V_{SO}/t$  and  $U = 0$  are shown in Fig. 4(c). In the first place,  $J_{SO,x}$  increases in general, as expected, with  $V_{SO}/t$ , for all the interval of  $\beta/\alpha$  considered except near the pure Rashba model for large  $V_{SO}/t$ , as it was reported before in Ref. [34]. More important is that for a fixed  $V_{SO}/t$ ,  $J_{SO,x}$  increases with  $\beta/\alpha$  and this behavior becomes most pronounced as  $V_{SO}/t$  increases. Overall, the behavior of  $J_{SO,x}$  with  $\beta/\alpha$  and  $V_{SO}/t$  follows very closely the one for  $D_{SO}$  shown in Fig. 2(a).

The effect of the Hubbard repulsion is in general, as it is well-known in correlated electron metallic systems, to suppress charge currents. This effect is already apparent in Fig. 4(b), for both the total current  $J_x$  and its  $J_{SO,x}$  contribution. A more systematic and quantitative study of the variation of  $J_{SO,x}$  with  $U$  as a function of  $\beta/\alpha$  and for  $V_{SO}/t = 0.6$ , is provided in Fig. 4(d). Indeed, as it can be seen in this Figure, the suppression of  $J_{SO,x}$  with  $U$  takes place up to the largest Hubbard repulsion considered,  $U = 8$ , while the system remains in its metallic state. The same behavior is observed for all values of  $V_{SO}/t$ .

Since the transversal spin current  $J_y^s$  involves differences between various terms (see Appendix B), in order to avoid large errors stemming from the separate time evolution of each of those terms, it is preferable to compute this current as a time derivative of the total  $S^z$  of the sites located on two rungs at the center of the strip and belonging to the same chain. In this way, the total  $J_y^s$  is computed but the separate information on  $J_{hop,y}^s$  and  $J_{SO,y}^s$  is lost. To examine the total  $J_y^s$  instead of the more relevant, according to the results obtained in linear

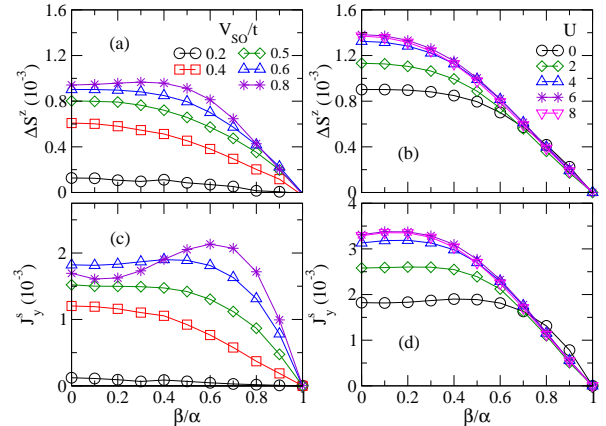


FIG. 5. (Color online) (a, b) Spin accumulation and (c, d)  $J_y^s$ , as a function of  $\beta/\alpha$ . (a, c) Results for various values of  $V_{SO}/t$  (symbols indicated on the plot) and  $U = 0$ . (b, d) Results for  $V_{SO}/t = 0.6$  and various values of  $U$  indicated on the plot. Results obtained with td-DMRG on the  $24 \times 2$  cluster.

response,  $J_{hop,y}^s$ , is in any case innocuous since the contribution from  $J_{SO,y}^s$  is always much smaller, as it will be discussed in Sec. V.

Results obtained by td-DMRG for the two most relevant properties in the context of the spin Hall effect, the transversal spin current  $J_y^s$  and the spin accumulation  $\Delta S^z$ , defined by Eq. (10), are shown in Fig. 5.

Let us start with the noninteracting case,  $U = 0$ . Results for  $\Delta S^z$  and  $J_y^s$  as a function of  $\beta/\alpha$ , for various  $V_{SO}/t$ , are shown in Figs. 5(a) and 5(c) respectively. In general, as expected, these quantities increase with  $V_{SO}/t$  for any value of  $\beta/\alpha$ . As for  $J_{SO,x}$ , a departure of this behavior can be observed for  $J_y^s$  near the Rashba limit and large  $V_{SO}/t$ , and the same behavior occurs for  $\sigma_{sH}$  in linear response (Fig. 1(a)). Another general behavior is the vanishing of  $J_y^s$  and  $\Delta S^z$  as  $\beta/\alpha$  approaches 1, that is as the system approaches the persistent helix state. This behavior is again expected since by switching  $\beta$  and  $\alpha$ ,  $J_y^s$  and  $\Delta S^z$  reverse their signs.

More importantly, it should be noticed that a non-monotonic behavior in  $J_y^s$  can be observed for  $V_{SO}/t \gtrsim 0.6$  in Fig. 5(c). This maximum is larger than error bars, which are of the order of the symbol sizes. The presence of this maximum, although much less pronounced, is consistent with the one reported previously for the spin Hall conductivity (Fig. 1). Taking into account the opposite trends in the variation with  $\beta/\alpha$  of  $J_{SO,x}$ , shown in Fig. 4(c) and of  $J_y^s$  (Fig. 5(b)), and since  $\sigma_{sH}$  involves the commutator between both quantities, one could speculate that a convolution of those behaviors would lead to the strong peak observed in  $\sigma_{sH}$  at an intermediate value of  $\beta/\alpha$ .

On the other hand, the behavior of  $\Delta S^z$  is monotonic between  $\beta = 0$  and  $\beta = \alpha$ . The very weak maximum observed for  $V_{SO}/t = 0.8$  certainly falls within the error bars of the calculation.

Let us now examine the evolution of these quanti-

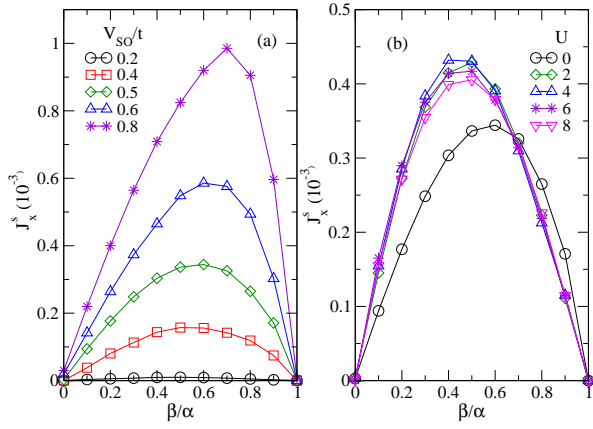


FIG. 6. (Color online) Longitudinal spin current  $J_x^s$ , as a function of  $\beta/\alpha$ , (a) for various values of  $V_{SO}/t$  (symbols indicated on the plot) and  $U = 0$ , (b) for  $V_{SO}/t = 0.5$  and various values of  $U$  indicated on the plot. Results obtained with td-DMRG on the  $24 \times 2$  cluster.

ties when the Hubbard interaction  $U$  is switched on. Figs. 5(b) and 5(d) show results for the spin accumulation and the transversal spin current, respectively, for  $V_{SO}/t = 0.6$ , and various values of  $U$ . In Fig. 5(b), the most noticeable feature is the systematic increase of  $\Delta S^z$  with  $U$  up to the maximum value considered,  $U = 8$ , in the whole interval of  $\beta/\alpha$ , with the constraint that  $\Delta S^z \rightarrow 0$  when  $\beta/\alpha \rightarrow 1$ . Notice that results for  $U = 6$  and  $U = 8$  are indistinguishable. This enhancement in  $\Delta S^z$  was observed for all the values of  $V_{SO}/t$  examined, thus extending the result obtained for the Rashba model [34] to the whole range of  $\beta/\alpha$ .

Similarly, as shown in Fig. 5(d),  $J_y^s$  also increases with  $U$ , again saturating at  $U \approx 8$ . Besides, the presence of a maximum of  $J_y^s$  at an intermediate value of  $\beta/\alpha$  is preserved by  $U$ . However, this maximum is smoothed out by  $U$  and its location is shifted to lower values of  $\beta/\alpha$ . This enhancement of  $J_y^s$  with  $U$  is observed for  $V_{SO}/t \leq 0.6$ , but for  $V_{SO}/t = 0.8$ ,  $J_y^s$  becomes actually suppressed by increasing  $U$ . Notice that, as said above, even for this value of  $V_{SO}/t$ , the spin accumulation is enhanced by  $U$ . Since  $J_{SO,x}$  is in general suppressed by  $U$ , while  $J_y^s$  is enhanced by  $U$ , the previously mentioned handwaving argument based on a convolution of  $J_{SO,x}$  and  $J_y^s$ , would not lead to a conclusive guess for the behavior of the spin Hall conductivity with  $U$ .

To end this section, let us examine the evolution of the longitudinal or polarized spin current,  $J_x^s$ , as a function of  $\beta/\alpha$ . The behavior of this quantity in this slightly out of equilibrium system should be compared with the one of  $\sigma_{xx}^s$  discussed in the previous section. In the same way as for the transversal spin current, in order to minimize errors,  $J_x^s$  is computed as the time derivative of the total  $S^z$  of the left half of the cluster. Again, the separate information of the hopping or SO contributions to  $J_x^s$  is lost but as discussed above, to analyze  $J_x^s$  instead of  $J_{hop,x}^s$  is relatively innocuous, and in any case, it is  $J_x^s$

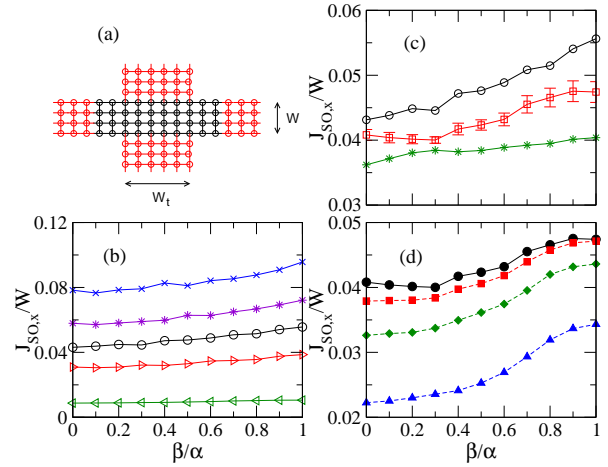


FIG. 7. (Color online) (a) Schematic illustration of the four terminal setup for the Landauer-Buttiker calculation. (b)  $J_{SO,x}$  per chain as a function of  $\beta/\alpha$  for  $V_{SO}/t = 0.2, 0.4, 0.5, 0.6$  and 0.8, from bottom to top, obtained for the  $80 \times 16$  cluster,  $U = 0$ . (c)  $J_{SO,x}/W$  for  $V_{SO}/t = 0.5$  and  $U = 0$ , obtained for the  $40 \times 4$ ,  $50 \times 8$ , and  $80 \times 16$  clusters from bottom to top. (d)  $J_{SO,x}/W$  for  $V_{SO}/t = 0.5$  and  $U = 0, 1, 2$ , and 4, from top to bottom, obtained for the  $50 \times 8$  cluster.

the quantity that is experimentally accessible.

Results for  $J_x^s$  as a function of  $\beta/\alpha$  for various values of  $V_{SO}/t$ ,  $U = 0$ , are shown in Fig. 6(a), where it could be observed that  $J_x^s$  follows roughly the same behavior as  $\sigma_{xx}^s$  shown in Fig. 3(a). In particular,  $J_x^s$  vanishes both at the Rashba point and at the PSH point. The more rounded-off dependence may be due to taking  $J_x^s$  instead of  $J_{hop,x}^s$ , and also due to the relatively small value of  $L$  and open BC adopted. In any case, it is clear that there is an asymmetric shape of  $J_x^s$ , and that, for  $V_{SO}/t = 0.8$ , there is a change of curvature at the maximum value around  $0.7 \leq \beta/\alpha \leq 0.8$ .

In Fig. 6(b), it can be seen that the longitudinal spin current is first *enhanced* by the Hubbard repulsion, reaching a maximum at  $U = 4$ , and then it is *suppressed* for larger values of  $U$ . That is, the behavior of  $J_x^s$  with  $U$  is similar to the one of the spin accumulation and the transversal spin current, but its dependence with  $U$  is different. This issue would deserve further study, increasing the precision and examining finite size effects, but this is out of reach of present computational capabilities,

## V. LANDAUER-BUTTIKER APPROACH

The setup of the system is schematically shown in Fig. 7(a). The horizontal leads and the central scattering region have width  $W$  and the two vertical transversal leads have width  $W_t$ . The four leads are semi-infinite and the central region has length  $L$ . The leads are numbered from 0 to 3 starting from the left horizontal lead and moving clockwise. A small voltage bias  $\Delta V_{02} = 0.1$  is applied between the horizontal leads, and

$\Delta V_{01} = \Delta V_{03} = \Delta V_{02}/2$ , which implies  $\Delta V_{13} = 0$ .

Fig. 7(b) shows results for the SO or spin flipping longitudinal charge current,  $J_{SO,x}$ , per chain, obtained on the  $80 \times 16$  central cluster for various values of  $V_{SO}/t$ , and  $U = 0$ . These results were obtained by averaging over  $W_t = 24, 32$  and  $40$ . The error bars due solely to this averaging procedure are shown for example for the  $50 \times 8$  central region in Fig. 7(c). In general,  $J_{SO,x}/W$  not only increases with  $V_{SO}/t$  for each  $\beta/\alpha$  but, what is more important, it increases with  $\beta/\alpha$  for a fixed  $V_{SO}/t$ . This behavior is more clear when a single value of  $V_{SO}/t$  is considered, as in Figs. 7(c) and 7(d).

In Fig. 7(c),  $J_{SO,x}/W$  is shown as a function of  $\beta/\alpha$ , for  $V_{SO}/t = 0.5$ , and for central clusters of varying width,  $W = 4, 8$ , and  $16$ . It can be observed not only an overall increase of  $J_{SO,x}/W$  with  $W$ , but also an increasing slope. This overall increase with  $W$  is consistent with the one obtained in linear response for  $D_{SO}$  (Fig. 2(d)). Results for the  $40 \times 4$  and  $50 \times 8$  central clusters have been obtained by averaging over  $W_t = 16, 24$  and  $32$ .

In Fig. 7(d),  $J_{SO,x}/W$  is shown for  $V_{SO}/t = 0.5$ , and various values of  $U$  on a  $50 \times 8$  cluster. As expected,  $J_{SO,x}/W$  decreases as  $U$  is increased, as it was observed for  $W = 2$  in Fig. 4(d), but the system remains metallic up to the largest value of the Hubbard repulsion considered,  $U = 4$ . The most relevant result is that the increasing trend of  $J_{SO,x}/W$  with  $\beta/\alpha$  is still clearly present up to  $U = 4$ .

Let us now consider the two quantities that are more relevant to the spin Hall effect, the spin accumulation and the transversal spin current, starting with the non-interacting case,  $U = 0$ . The central system is a  $200 \times 8$  cluster. The error bars, shown in Figs. 8(a) and 8(b) for the two extreme values of  $V_{SO}/t$  considered, again only correspond to the averaging over three different widths of the transversal leads,  $W_t = 24, 40$  and  $80$ . For these two physical properties, the error bars are much larger than the ones for  $J_{SO,x}$ .

Results for  $\Delta S^z$  as a function of  $\beta/\alpha$  for various values of  $V_{SO}/t$  are shown in Fig. 8(a). By neglecting some oscillations that are not significant within the errors of the calculation, it can be seen that the main trends are that  $\Delta S^z$  decreases monotonically for a given value of  $V_{SO}/t$  as a function of  $\beta/\alpha$ , vanishing at the PSH point, and increases at each value of  $\beta/\alpha$  by increasing  $V_{SO}/t$ . These behaviors are similar to those for the  $W = 2$  strip obtained by td-DMRG and shown in Fig. 5(a).

More interesting are the results for the transversal spin current,  $J_y^s$ , shown in Fig. 8(b). In this case there is clear nonmonotonic behavior characterized by a maximum of  $J_y^s$  that is located at values of  $\beta/\alpha$  that increase with  $V_{SO}/t$ . The presence of this maximum in  $J_y^s$  confirms the behavior shown in Fig. 5(c) for  $W = 2$ , and is consistent with the one for  $\sigma_{sH}$  depicted in Fig. 1. Also notice that the hopping part of  $J_y^s$  is in general larger than the SO part, and these two contributions have the same sign, as shown in Fig. 8(b). In the Rashba limit,  $\beta = 0$ ,  $J_{SO,y}^s$  is strictly equal to zero for all  $V_{SO}/t$ , in agreement with

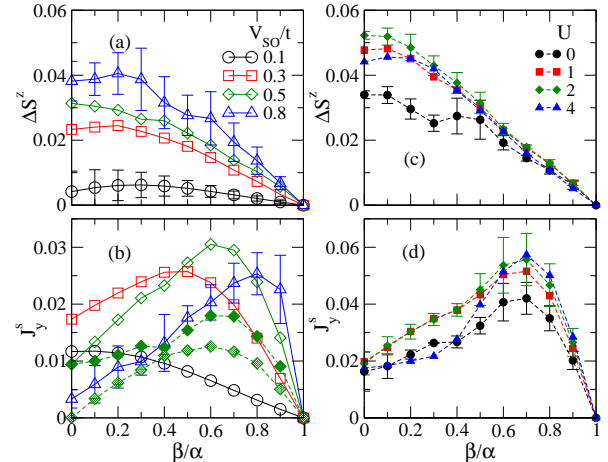


FIG. 8. (Color online) (a) Spin accumulation and (b) total transversal spin current on the  $200 \times 8$  cluster, as a function of  $\beta/\alpha$  for various values of  $V_{SO}/t$  as indicated on the plot (open symbols, solid lines). (c) Spin accumulation and (d) total transversal spin current for  $V_{SO}/t = 0.5$  for various values of  $U$  indicated on the plot, on the  $50 \times 8$  cluster. In (b) the hopping (full diamonds, dashed line) and SO (shaded diamonds, dotted line) contributions to  $J_y^s$  for  $V_{SO}/t = 0.5$  have been added. Results obtained by the Landauer-Buttiker formalism.

previous results [42] and consistently with the results for  $\sigma_{sH}$  where the solely contributing matrix elements are those of the operator  $\hat{j}_{hop,x}^s$ .

Let us now examine the effects of the Hubbard repulsion  $U$ . The error bars of the Landauer-Buttiker part of the calculation were obtained as before, but in this case to these errors one should have to add the ones coming from the Hartree-Fock procedure. The latter are difficult to estimate but they certainly increase with  $U$ . Results for the spin accumulation  $\Delta S^z$  on the  $50 \times 8$  central scattering region for  $V_{SO}/t = 0.5$  are depicted in Fig. 8(c). The most remarkable behavior is the enhancement of  $\Delta S^z$  with  $U$ , in all the range of  $\beta/\alpha$ , thus complementing the td-DMRG results for  $W = 2$  shown in Fig. 5(c). The maximum value of  $\Delta S^z$  is reached at  $U = 2$ . Taking into account the likely error bars of the calculation one could conclude that the behavior of  $\Delta S^z$  as a function of  $\beta/\alpha$  remains monotonic up to the largest value of  $U$  here considered.

Results for the transversal spin current  $J_y^s$  are shown in Fig. 8(d) for  $V_{SO}/t = 0.5$  and various values of  $U$  on the  $50 \times 8$  scattering region. First, notice that the nonmonotonic behavior observed for  $U = 0$  is still present up to  $U = 4$ , surviving the large error bars of the calculation. Again, the most interesting behavior is the enhancement of  $J_y^s$  with  $U$ , particularly in the region near the maximum point. For  $U = 4$ , there is a suppression of  $J_y^s$  at small values of  $\beta/\alpha$ . This suppression could be traced to the behavior of  $J_{SO,y}^s$  acquiring a *opposite* sign to that of  $J_{hop,y}^s$  for this value of  $U$ . This overall enhancement of  $J_y^s$  with  $U$  for  $W = 8$  complements the result for  $W = 2$

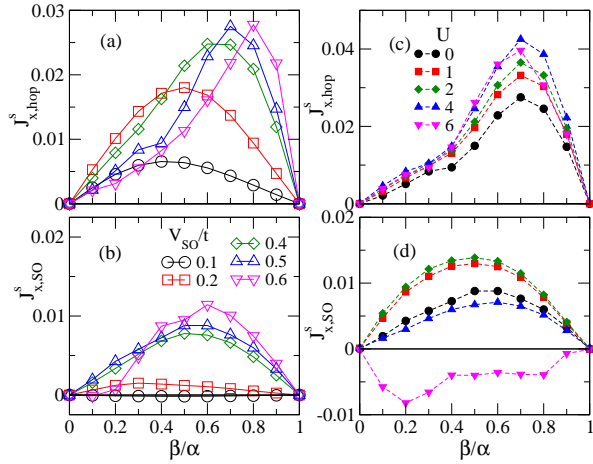


FIG. 9. (Color online) Longitudinal spin current on the  $50 \times 8$  cluster, as a function of  $\beta/\alpha$ . (a) Hopping contribution and (b) SO contribution for various values of  $V_{SO}/t$  as indicated on the plot. (c) Hopping contribution and (d) SO contribution for  $V_{SO}/t = 0.5$  and various values of  $U$  indicated on the plot. Results obtained by Landauer-Buttiker calculation.

obtained with td-DMRG shown in Fig. 5(d),

To end this section, let us study the longitudinal polarized spin current  $J_x^s$  on the  $50 \times 8$  central region. The hopping,  $J_{hop,x}^s$ , and SO,  $J_{SO,x}^s$ , contributions are shown in Figs. 9(a) and (b) respectively, as a function of  $\beta/\alpha$  and for various values of  $V_{SO}/t$ ,  $U = 0$ . As argued before,  $J_x^s$ , as well as its two contributions,  $J_{hop,x}^s$  and  $J_{SO,x}^s$ , vanish at the pure Rashba point and at the PSH point. Between these two limits, both contributions to  $J_x^s$  acquire finite values. It can be seen in Fig. 9(a) that  $J_{hop,x}^s$ , for a given value of  $V_{SO}/t$ , follows qualitatively the same behavior as  $\sigma_{xx}^s$  for the same strip width  $W = 8$  (Fig. 3(c)), that is, it varies smoothly for small values of  $V_{SO}/t$ , and then it develops a more pronounced maximum for larger  $V_{SO}/t$ . This maximum becomes a peak for  $V_{SO}/t \geq 0.5$ , separating two regions with clearly different behaviors. In addition, the position of this maximum,  $R^*$ , shifts to higher  $\beta/\alpha$  as  $V_{SO}/t$  increases. Moreover, it should be noticed that  $R^*$  coincides with the corresponding one of the transversal spin current for the same value of  $V_{SO}/t$ , as shown in Fig. 8, and again this is consistent with the behavior of  $\sigma_{xx}^s$  and  $\sigma_{sH}$ , where the values of  $R^*$  were also coincident.

In contrast, as shown in Fig. 9(b), the SO part of  $J_x^s$  is much smaller than the hopping part, and its behavior is smoother. Hence, the more relevant contribution to  $J_x^s$  is of the hopping type, and this result is consistent with the linear response result indicating that the most relevant contribution to the longitudinal spin conductivity is due to the correlation between  $\hat{j}_{SO,x}$  and  $\hat{j}_{hop,x}^s$ .

It is also important to notice that, as shown in Fig. 9(c), similarly to what was found for the spin accumulation and the transversal spin current (Figs. 8(c) and 8(d)),  $J_{hop,x}^s$  is enhanced by the Hubbard repulsion

$U$ , up to  $U = 4$ . Besides,  $U$  preserves the overall dependence of  $J_{hop,x}^s$  with  $\beta/\alpha$ . In contrast,  $J_{SO,x}^s$ , shown in Fig. 9(d) is enhanced up to  $U = 2$  and becomes suppressed by larger values of  $U$ , even becoming negative for  $U = 6$ , that is acquiring an opposite direction to  $J_{hop,x}^s$ .

## VI. CONCLUSIONS

In this work, three different techniques that cover different equilibrium and out-of equilibrium regimes, interacting and noninteracting systems, and ranges of strip widths, were employed to study magneto-transport properties due to combined Rashba and Dresselhaus spin-orbit couplings.

The first main result is an unexpected nonmonotonic behavior as a function of the ratio of Dresselhaus to Rashba couplings,  $\beta/\alpha$ , in the spin Hall conductivity, calculated in linear response, and in the related transversal spin current,  $J_y^s$ , calculated within the td-DMRG and Landauer-Buttiker approaches. This nonmonotonic behavior is characterized by the presence of a maximum that separates regions with different curvatures. This maximum has the characteristic of a peak for small strip widths  $W$ , evolving into a cusp for larger  $W$ . A peak is also present in the longitudinal spin conductivity, and it is located at the same value of  $\beta/\alpha$  as the peak in the spin Hall conductivity for the corresponding values of the SOI strength and  $W$ . Again, a maximum separating asymmetric regions with different behavior was observed in the related longitudinal spin current,  $J_x^s$ . Moreover, these maxima in  $J_x^s$  are located at the same value of  $\beta/\alpha$  as the ones of  $J_y^s$  for the same set of parameters. Notice that for this result to make sense, the strip width and the ratio of SOI,  $\beta/\alpha$ , have to be independent variables, which excludes the possibility of the strips to be defined by electrical gates.

The second major result of the present effort is the enhancement of the main physical properties related to the spin Hall effect, the spin accumulation and the transversal spin current, as well as the longitudinal spin current, under the application of a Hubbard on-site repulsion with coupling  $U$ . This enhancement is present up to a relatively high value of  $U$ , depending on the physical property, beyond which this property saturates or starts to decrease.

To have sizable electron correlations, the main candidate materials for building the strips could be transition metal oxides, such as  $\text{SrTiO}_3$ , mentioned in the Introduction, where the presence of SOI is ubiquitous. In addition, strips of arbitrarily width could be edged from the surfaces or interfaces involving these compounds with orthorhombic structure. Of course, the region at the surfaces or interfaces where itinerant SO processes take place is not a mathematical plane but it has a finite depth, and it is not trivial to determine to what extent the electron correlations due to d-orbitals are significant nor if the density of carriers is large enough for such cor-

relations to have some effect (on magnetic properties for instance). Although a full investigation of the influence of the electron filling is out of the scope of the present work, it would be important to study other compounds where electron correlations, large spin-orbit coupling and finite carrier density could be present. One of these new compounds could be the orthorhombic perovskite iridate,  $\text{SrIrO}_3$ , which is a three-dimensional semimetal, and where the spin Hall effect has been observed [55], although Rashba or Dresselhaus types of SOC have not yet been identified. Another candidate material is  $\text{Sr}_3\text{Ir}_2\text{O}_7$  lying close to the metal-Mott insulator transition and exhibiting weak metallicity [56].

Finally, together with the study of varying electron filling, future effort should be devoted to correlate the presently shown behavior of the spin Hall conductivity and spin currents, with the behavior of magnetic properties, as it was for instance performed for the Rashba-Hubbard model in the two-chain strip [34]. For the isotropic 2D system, a study relating the spin conductivities with dynamical magnetic susceptibilities was done in Ref. [57] but its extension to the presently studied system is certainly out of the scope of the present work.

## ACKNOWLEDGMENTS

The author wishes to thank A. Greco, I. Hamad, and L. Lara, for useful discussions, and C. Gazza for helping to understand and write the KWANT code. The author is partially supported by the Consejo Nacional de Investigaciones Científicas y Técnicas (CONICET) of Argentina, through CONICET-PIP No. 11220120100389CO.

## Appendix A: Rashba and Dresselhaus Hamiltonians

The Rashba SO Hamiltonian in the square lattice is obtained from:

$$H_R = \alpha \sum_l [(c_{l+y,\uparrow}^\dagger c_{l+y,\downarrow}^\dagger)(i\sigma^x) \begin{pmatrix} c_{l,\uparrow} \\ c_{l,\downarrow} \end{pmatrix} - (c_{l+x,\uparrow}^\dagger c_{l+x,\downarrow}^\dagger)(i\sigma^y) \begin{pmatrix} c_{l,\uparrow} \\ c_{l,\downarrow} \end{pmatrix} + H.c.] \quad (\text{A1})$$

The Dresselhaus SO Hamiltonian  $H_D$  results from a similar expression just by interchanging  $c_{l+y,\sigma}^\dagger c_{l+y,\sigma}$  with  $c_{l+x,\sigma}^\dagger c_{l+x,\sigma}$ .

Assuming translational invariance along the  $x$ -axis, the SO part of the Hamiltonian in momentum space can be

written as:

$$H_R + H_D = \sum_{\mathbf{k}} \begin{pmatrix} A & B \\ B^* & A \end{pmatrix} \quad (\text{A2})$$

where  $A(k_x)$  and  $B(k_x)$  are  $W \times W$  matrices.

## Appendix B: Current operators

From the hopping term of the Hamiltonian,  $H_h$ , the following charge current operators are obtained [37]:

$$\hat{j}_{\sigma,l,\mu} = -it(c_{l+\mu,\sigma}^\dagger c_{l,\sigma} - c_{l,\sigma}^\dagger c_{l+\mu,\sigma}), \quad (\text{B1})$$

$\mu = x, y$ , and the following spin current operators:

$$\hat{j}_{l,\mu}^s = \frac{t}{2}(\hat{j}_{\uparrow,l,\mu} - \hat{j}_{\downarrow,l,\mu}). \quad (\text{B2})$$

From the SO terms of the Hamiltonian,  $H_R$  and  $H_D$ , the following charge current operators are derived:

$$\begin{aligned} \hat{j}_{SO,l,x} &= \hat{j}'_{SO,l,x} + \hat{j}''_{SO,l,x} \\ \hat{j}_{SO,l,y} &= \hat{j}'_{SO,l,y} + \hat{j}''_{SO,l,y} \end{aligned}$$

and the following spin current operators:

$$\begin{aligned} \hat{j}_{SO,l,x}^s &= \frac{1}{2}(\hat{j}'_{SO,l,x} - \hat{j}''_{SO,l,x}) \\ \hat{j}_{SO,l,y}^s &= \frac{1}{2}(\hat{j}'_{SO,l,y} - \hat{j}''_{SO,l,y}) \end{aligned}$$

where the spin-selected SO charge currents are:

$$\begin{aligned} \hat{j}'_{SO,l,x} &\equiv \hat{j}_{SO,\uparrow\rightarrow\downarrow,l,x} = i(\hat{h}_{SO,2,l,x} - \hat{h}_{SO,2,l,-x}) \\ \hat{j}''_{SO,l,x} &\equiv \hat{j}_{SO,\downarrow\rightarrow\uparrow,l,x} = i(\hat{h}_{SO,1,l,x} - \hat{h}_{SO,1,l,-x}) \\ \hat{j}'_{SO,l,y} &\equiv \hat{j}_{SO,\uparrow\rightarrow\downarrow,l,y} = i(\hat{h}_{SO,4,l,y} - \hat{h}_{SO,4,l,-y}) \\ \hat{j}''_{SO,l,y} &\equiv \hat{j}_{SO,\downarrow\rightarrow\uparrow,l,y} = i(\hat{h}_{SO,3,l,y} - \hat{h}_{SO,3,l,-y}) \end{aligned}$$

and the SO Hamiltonian terms are defined as:

$$\begin{aligned} \hat{h}_{SO,1,l,-x} &= -(\alpha, \beta) c_{l,\downarrow}^\dagger c_{l+x,\uparrow} \\ \hat{h}_{SO,2,l,x} &= (\alpha, \beta) c_{l+x,\downarrow}^\dagger c_{l,\uparrow} \\ \hat{h}_{SO,3,l,-y} &= -(\beta, \alpha) c_{l,\downarrow}^\dagger c_{l+y,\uparrow} \\ \hat{h}_{SO,4,l,y} &= (\beta, \alpha) c_{l+y,\downarrow}^\dagger c_{l,\uparrow} \\ \hat{h}_{SO,2,l,-x} &= (\alpha, -\beta) c_{l,\uparrow}^\dagger c_{l+x,\downarrow} \\ \hat{h}_{SO,1,l,x} &= (-\alpha, \beta) c_{l+x,\uparrow}^\dagger c_{l,\downarrow} \\ \hat{h}_{SO,4,l,-y} &= (\beta, -\alpha) c_{l,\uparrow}^\dagger c_{l+y,\downarrow} \\ \hat{h}_{SO,3,l,y} &= (-\beta, \alpha) c_{l+y,\uparrow}^\dagger c_{l,\downarrow} \end{aligned}$$

.

---

[1] Y. Ando, J. Phys. Soc. Jpn. **82**, 102001 (2013).

[2] G. A. Prinz, Science **282**, 1660 (1998).

[3] S. A. Wolf, D.D. Awschalom, R.A. Buhrman, J.M. Daughton, S. von Molnar, M.L. Roukes, A.Y. Chtchelkina, D.M. Treger, Science **294**, 1488 (2001).

[4] I. Zutic, J. Fabian, and S. Das Sarma, Rev. Mod. Phys. **76**, 323, (2004).

[5] G. Dresselhaus, Phys. Rev. **100**, 580 (1955).

[6] E. I. Rashba, Sov. Phys. Solid State **2**, 1109 (1960); Y. A. Bychkov and E. I. Rashba, JETP Lett. **39**, 78 (1984).

[7] A. Manchon, H. C. Koo, J. Nitta, S. M. Frolov, and R. A. Duine, Nature Mater. **14**, 871 (2015).

[8] S. D. Ganichev and L. E. and Golub, Phys. Status Solidi B **251** 1801 (2014).

[9] S. D. Ganichev, M. Trushin, and J. Schliemann, *Spin Polarization by Current in Handbook of Spin Transport and Magnetism*, edited by E. Y. Tsymbal and I. Zutic, (Chapman and Hall/CRC, 2012).

[10] F. Herzog, H. Hardtdegen, T. Schpers, D. Grundler, and M. A. Wilde, New J. Phys. **19**, 103012 (2017).

[11] D. Rainis and D. Loss, Phys. Rev. B **90**, 235415 (2014).

[12] S. Anghel, F. Passmann, A. Singh, C. Ruppert, A. V. Poshakinskiy, S. A. Tarasenko, J. N. Moore, G. Yusa, T. Mano, T. Noda, X. Li, and M. Betz, 1708.09150, Phys. Rev. B **xx**

[13] B. A. Bernevig, J. Orenstein, and S. C. Zhang, Phys. Rev. Lett. **97**, 236601 (2006).

[14] P. Wenk and S. Kettemann, Phys. Rev. B **81**, 125309 (2010).

[15] F. Dettwiler, J. Fu, S. Mack, P. J. Weigle, J. C. Egues, D. D. Awschalom, and D. M. Zumbühl, Phys. Rev. X **7**, 031010 (2017).

[16] J. Schliemann, J.C. Egues, D. Loss, Phys. Rev. Lett. **90**, 146801 (2003).

[17] M. Kohda, V. Lechner, Y. Kunihashi, T. Dollinger, P. Olbrich, C. Schönhuber, I. Caspers, V. V. Belkov, L. E. Golub, D. Weiss, K. Richter, J. Nitta, and S. D. Ganichev, Phys. Rev. B **86**, 081306(R) (2012).

[18] Z. Li, F. Marsiglio, and J. P. Carbotte, Sci. Rep. **3**, 2828 (2013).

[19] J. Sinova, D. Culcer, Q. Niu, N. A. Sinitsyn, T. Jungwirth, and A. H. MacDonald, Phys. Rev. Lett. **92**, 126603 (2004).

[20] E. I Rashba, Phys. Rev. B **70**, 201309 (2004).

[21] S. Q. Shen, Phys. Rev. B **70**, 081311 (2004).

[22] C. H. Chang, J. Tsai, H. F. Lo, and A. G. Malshukov, Phys. Rev. B **79**, 125310 (2009).

[23] P. Altmann, M. P. Walser, C. Reichl, W. Wegscheider, and G. Salis, Phys. Rev. B **90**, 201306 (R) (2014).

[24] A. Sasaki, S. Nonaka, Y. Kunihashi, M. Kohda, T. Bauernfeind, T. Dollinger, K. Richter, and J. Nitta, Nature Nanotechnology **9**, 703 (2014).

[25] M. H. Liu, S.-H. Chen, and C.-R. Chang, Phys. Rev. B **78**, 165316 (2008).

[26] H. Y. Hwang, Y. Iwasa, M. Kawasaki, B. Keimer, N. Nagaosa, and Y. Tokura, Nature Mater. **11**, 103 (2012).

[27] A. D. Caviglia, M. Gabay, S. Gariglio, N. Reyren, C. Cancellieri, and J.-M. Triscone , Phys. Rev. Lett. **104**, 126803 (2010).

[28] S. Banerjee, O. Erten and M. Randeria, Nature Phys. **9**, 626 (2013).

[29] K. Gopinadhan, A. Annadi, Y. Kim, A. Srivastava, Arriando, and T. Venkatesan, Adv. Electron. Mater. **1**, 1500114 (2015).

[30] S. Caprara, F. Peronaci, and M. Grilli, Phys. Rev. Lett. **109**, 196401 (2012).

[31] G. Khalsa, B. Lee, and A. H. MacDonald, Phys. Rev. B **88** 041302, (2013).

[32] D. Bucheli, M. Grilli, F. Peronaci, G. Seibold, and S. Caprara, Phys. Rev. B **89** 195448, (2014).

[33] J. Ruhman, A. Joshua, S. Ilani and E. Altman, Phys. Rev. B **90**, 125123 (2014).

[34] J. A. Riera, Phys. Rev. B **88**, 045102 (2013).

[35] F. Goth and F. F. Assaad, Phys. Rev. B **90**, 195103 (2014).

[36] A. N. Kocharyan, G. W. Fernando, K. Fang, K. Pandage, and A. V. Balatsky, AIP Advances **6**, 055711 (2016).

[37] I. J. Hamad, C. J. Gazza, and J. A. Riera, Phys. Rev. B **93**, 205113 (2016).

[38] F. Sun, J. Ye, and W.-M. Liu, New J. Phys. **19**, 063025 (2017).

[39] T. P. Pareek and P. Bruno, Phys. Rev. B **65**, 241305 (2002).

[40] X. Xiao and Y. Chen, Europhys. Lett. **90**, 47004 (2010).

[41] J. Zelezny, H. Gao, K. Vyborny, J. Zemen, J. Masek, A. Manchon, J. Wunderlich, J. Sinova, and T. Jungwirth, Phys. Rev. Lett. **113**, 157201 (2014).

[42] J. A. Riera, Phys. Rev. B **95**, 045146 (2017).

[43] The contribution of the mixing term is also equal to zero for Rashba-Dresselhaus conducting strips coupled to ferromagnetic layer, J. A. Riera, in preparation (2017).

[44] U. Schollwöck, Rev. Mod. Phys. **77**, 259 (2005).

[45] P. Schmitteckert, Phys. Rev. B **70**, 121302(R), (2004).

[46] K. A. Al-Hassanieh, A. E. Feiguin, J. A. Riera, C. A. Busser, and E. Dagotto, Phys. Rev. B **73**, 195304 (2006).

[47] C. W. Groth, M. Wimmer, A. R. Akhmerov, X. Waintal, *Kwant: a software package for quantum transport*, New J. Phys. **16**, 063065 (2014).

[48] Actually, the energy of the scattering region was varied between  $E_F - 0.04$ , and  $E_F + 0.04$ .

[49] B. K. Nikolić, S. Souma, L. P. Zárbo, and J. Sinova, Phys. Rev. Lett. **95**, 046601 (2005).

[50] P.-H. Chang, F. Mahfouzi, N. Nagaosa, and B. K. Nikolić, Phys. Rev. B **89**, 195418 (2014).

[51] T. Giamarchi and C. Lhuillier, Phys. Rev. B **43**, 12943 (1991).

[52] N. Nagaosa, J. Sinova, S. Onoda, A. H. MacDonald, Rev. Mod. Phys. **82**, 1539 (2010).

[53] J. I. Inoue, G. E. W. Bauer, L. W. Molenkamp, Phys. Rev. B **67**, 033104 (2003).

[54] V. P. Amin, M. D. Stiles, Phys. Rev. B **94**, 104419 (2016).

[55] A. S. Patri, K. Hwang, H.-W. Lee, Y. B. Kim, preprint arXiv:1711.00861 (2017).

[56] C. Liu, S.-Y. Xu, N. Alidoust, T.-R. Chang, H. Lin, C. Dhital, S. Khadka, M. Neupane, I. Belopolski, G. Landolt, H.-T. Jeng, R. S. Markiewicz, J. H. Dil, A. Bansil, S. D. Wilson, and M. Z. Hasan, Phys. Rev. B **90**, 045127 (2014).

[57] S. I. Erlingsson, J. Schliemann, and D. Loss, Phys. Rev. B **71**, 035319 (2005).